

A Unified Leader-Follower Scheme for Mobile Robots with Uncalibrated On-board Camera

Dejun Guo, *Student Member, IEEE*, Hesheng Wang, *Senior Member, IEEE*, Weidong Chen, *Member, IEEE*, Ming Liu, *Member, IEEE*, Zeyang Xia, *Senior Member, IEEE*, and Kam K. Leang, *Member, IEEE*

Abstract—This paper studies the problem of image-based leader-follower formation control for mobile robots, where the controller is designed independently of the leader's motion. An adaptive control scheme, which is suitable for both omnidirectional and perspective cameras, is proposed. The proposed approach avoids the need for accurate calibration of the extrinsic parameters of the omnidirectional camera as well as the intrinsic and extrinsic parameters of perspective camera. Additionally, the coefficients of the plane where the feature point moves relative to the camera frame can be uncertain. These uncertain constant parameters are estimated using an adaptive estimator. Uniform Semi-global Practical Asymptotic Stability (USPAS) of the system is shown using the Lyapunov approach. Experimental results are presented to demonstrate the effectiveness of the proposed control scheme.

Index Terms—Adaptive control, mobile robot, visual servoing.

I. INTRODUCTION

Formation control of mobile robots is an active area of research because of its potential in a wide variety of civil and military applications, for example in surveillance, search and rescue, transportation, and law enforcement. In the leader-follower approach, one robot is considered as the formation leader, and the other robots, referred to as the followers, maintain a desired relative position with the leader and each other. Various approaches have been presented and studied extensively for the leader-follower problem [1-8]. In particular, many leader-follower approaches for mobile robots have been developed based on the relative pose. However, one way to obtain relative pose is through on-board sensing such as LiDAR, which can be expensive. On the other hand, the relative pose can be obtained using an on-board calibrated omnidirectional camera [1]. Likewise, pose

reconstruction can be achieved using an on-board calibrated perspective camera [2], but unfortunately the pose reconstruction process can be time-consuming and calibration error can lead to reduced accuracy. In addition, a vision-based position estimator was proposed by considering the stability of the whole system [3].

A more effective leader-follower scheme can be achieved by locking in on the desired position of the leader within the field of view and avoiding the need to accurately measure the relative pose and velocity of the leader. Thus, image information can be exploited for leader-follower formation control, resulting in image-based visual-servoing.

In [4] and [5], the proposed controllers depended on the image information from an omnidirectional camera and a perspective camera, respectively. The proposed methods also relied on the image position of a static point on the ground and the leader's velocity. Additionally, the methods presented in [1-5] demanded that the camera's intrinsic and extrinsic parameters should be accurately calibrated.

It is pointed out that camera calibrations for a multi-robot system can be challenging. Several approaches avoid camera calibrations in the visual-servo task [6-8]. For example, in [6] and [7], the relative distance was estimated by an extended Kalman filter and immersion and invariance based estimator, respectively. The leader's velocity was determined through communication. An adaptive control scheme [8] and adaptive-repetitive control scheme [9] were proposed to handle the uncertain perspective camera parameters for formation control and trajectory tracking. In summary, limited work have been done to address the leader-follower approach using an uncalibrated on-board camera and without knowledge of the leader's velocity.

In this paper, a unified adaptive image-based leader-follower formation controller is proposed for mobile robots where either an omnidirectional or perspective on-board camera can be used. Additionally, either the extrinsic parameters of omnidirectional camera or both the intrinsic and extrinsic parameters of perspective camera can be uncertain. The coefficients of the plane where the feature point moves relative to the camera frame can also be uncertain. Additionally, it is assumed that the leader's velocity cannot be obtained by communication. Thus, an adaptive estimator is proposed to determine in real-time the uncertain constant parameters. The controller is designed based on the estimated parameters and an image-based filter used to compensate for the lack knowledge of leader's velocity. The Lyapunov method is used to prove the Uniform Semiglobal Practical Asymptotic Stability of the image error and the formation error. Finally, the adaptive image-based controller and the estimator are implemented on experimental mobile robots to demonstrate the controller's effectiveness.

*This work was supported in part by the Natural Science Foundation of China under Grant U1613218, 61473191, 61503245, in part by Shanghai Sailing Program under Grant 15YF1406300, in part by State Key Laboratory of Robotics and System (HIT). Corresponding Author: Hesheng Wang.

D. Guo and K. K. Leang are with the DARC (Design, Automation, Robotics & Control) Lab, University of Utah Robotics Center, Salt Lake City, Utah 84112, USA.

H. Wang (E-mail: wanghesheng@sjtu.edu.cn) and W. Chen are with the Department of Automation, Shanghai Jiao Tong University, Shanghai 200240, China and the Key Laboratory of System Control and Information Processing, Ministry of Education of China. H. Wang is also with State Key Laboratory of Robotics and System (HIT).

M. Liu is with Department of Electronics and Computer Engineering, Hong Kong University of Science and Technology, Hong Kong, China.

Z. Xia is with Institute of Biomedical and Health Engineering and Key Laboratory of Human-Machine Intelligence-Synergy Systems, Shenzhen Institutes of Advanced Technology, Chinese Academy of Sciences, Shenzhen, China.

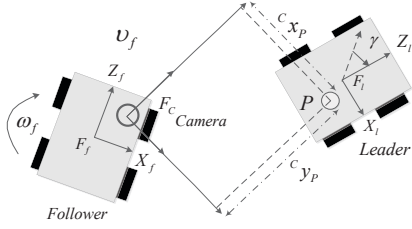


Fig. 1. Leader-follower system with an on-board camera.

II. PROBLEM FORMULATION

A. Problem Statement

The coordinate frames are defined as shown in Fig. 1. The origins of the follower frame, $F_f: \{O_f: X_f, Y_f, Z_f\}$, and the leader frame, $F_l: \{O_l: X_l, Y_l, Z_l\}$, are located at the center of rotation of the follower and the leader, respectively. The on-board camera could be either an omnidirectional camera or a perspective camera. The unified camera frame is defined by $F_c: \{O_c: X_c, Y_c, Z_c\}$.

Problem: Given a desired position on the image plane, the objective is to design a kinematic controller that guarantees the feature point on the leader converges asymptotically to the desired position on the image plane.

Assumptions: (1) The extrinsic parameters of the omnidirectional camera or the intrinsic and extrinsic parameters of the perspective camera, the position of the feature point relative to the camera, and the velocity of the leader are all assumed to be uncertain. (2) The mobile robots move in the ground plane. (3) The linear velocity of the leader is non-zero. (4) The feature point is in the field of view of the camera at all the times. (5) The motion plane of feature point does not pass through the optical center of perspective camera. (6) The linear and angular velocities of the leader are bounded by \bar{v}_l and $\bar{\omega}_l$.

Notation: For convenience, notations used in paper are listed as follows: $\|\cdot\|$ denotes the Euclidean norm of vectors. The bold face variable denotes a vector or matrix. The left superscript denotes the frame where a physical quantity is expressed in.

B. Camera Model

The unified mapping for cameras is introduced, where the two specific cases – the perspective camera model and the omnidirectional camera model – are explained.

Define the unified mapping $\rho(\bullet): \mathbb{R}^3 \rightarrow \mathbb{R}^2$ that maps the coordinates of 3D feature point P w.r.t. the unified camera frame, i.e., ${}^c\mathbf{P}_p \in \mathbb{R}^3$, to the coordinates of feature point P on the image plane, i.e., ${}^l\mathbf{P}_p \in \mathbb{R}^2$. This map can be expressed as

$${}^l\mathbf{P}_p = \rho({}^c\mathbf{P}_p). \quad (1)$$

Next, define the second unified mapping for cameras by $\delta(\bullet, \bullet): \mathbb{R}^2 \times \mathbb{R} \rightarrow \mathbb{R}^3$. Finally, define the third entry in ${}^c\mathbf{P}_p$ by ${}^{c_z}z_p$ which denotes the coordinate of feature point P in Z_c , i.e., the depth. δ maps ${}^l\mathbf{P}_p$ and the depth ${}^{c_z}z_p$ to ${}^c\mathbf{P}_p$, and it can be expressed as

$${}^c\mathbf{P}_p = \delta({}^l\mathbf{P}_p, {}^{c_z}z_p). \quad (2)$$

The unified mapping ρ and δ can be applied to either the perspective projection model or the omnidirectional camera

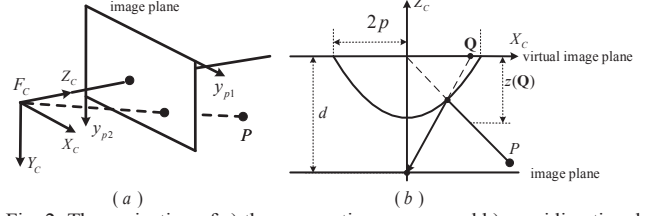


Fig. 2. The projection of a) the perspective camera and b) omnidirectional camera.

model. Such unified mapping will be used in the design of control scheme.

B.1. Perspective Camera Model

The perspective camera is simplified to a pin-hole camera with perspective projection. Figure 2(a) shows the projection model of the perspective camera. Here, ${}^l\mathbf{P}_p$ indicates $\mathbf{y}_p = [y_{p1} \ y_{p2}]^T$, the coordinates of feature point on the image plane. The unified mapping ρ in Eq. (1) can be expressed as

$$\mathbf{y}_p = \frac{1}{{}^{c_z}z_p} \begin{bmatrix} 1 & 0 & 0 \\ 0 & 1 & 0 \end{bmatrix} \mathbf{A} {}^c\mathbf{P}_p, \quad (3)$$

where ${}^{c_z}z_p$ denotes the depth of the feature point P expressed in F_c . \mathbf{A} is the intrinsic matrix which is given by

$$\mathbf{A} = \begin{bmatrix} \lambda_1 & 0 & y_{1o} \\ 0 & \lambda_2 & y_{2o} \\ 0 & 0 & 1 \end{bmatrix}. \quad (4)$$

Next, δ in Eq. (2) can be written as

$${}^c\mathbf{P}_p = {}^{c_z}z_p \mathbf{A}^{-1} \begin{bmatrix} \mathbf{y}_p \\ 1 \end{bmatrix}. \quad (5)$$

B.2. Omnidirectional Camera Model

The omnidirectional camera here includes a hyperbolic mirror and a pin-hole camera with perspective projection [11]. Figure 2(b) shows the projection model of the omnidirectional camera. Define a virtual image plane at the top of the mirror, and the coordinate of the feature point on this plane is $\mathbf{Q} = [q_1 \ q_2]^T$. Let the coordinate of the feature point on the image plane be $\mathbf{y}_o \in [y_{o1} \ y_{o2}]^T$. Then there exists a one-to-one mapping from \mathbf{Q} to \mathbf{y}_o , i.e.,

$$\begin{bmatrix} \mathbf{y}_o \\ 1 \end{bmatrix} = \mathbf{A} \begin{bmatrix} \mathbf{Q} \\ 1 \end{bmatrix}, \quad (6)$$

where \mathbf{A} is the intrinsic matrix of the pin-hole camera and is same as Eq. (4). Here, ${}^l\mathbf{P}_p$ indicates $\mathbf{Q} = [q_1 \ q_2]^T$. The unified mapping in Eq. (1) can be expressed as

$$\mathbf{Q} = \frac{1}{\lambda({}^c\mathbf{P}_p)} \begin{bmatrix} 1 & 0 & 0 \\ 0 & 1 & 0 \end{bmatrix} {}^c\mathbf{P}_p, \quad (7)$$

where $\lambda({}^c\mathbf{P}_p) = (-{}^{c_z}z_p + \xi \sqrt{{}^c x_p^2 + {}^c y_p^2 + {}^{c_z}z_p^2}) / \mu$. $\xi = d / \sqrt{d^2 + 4p^2}$ and $\mu = 2dp / \sqrt{d^2 + 4p^2}$ are the parameters of the mirrors [4][11]. The definitions of d and p are described in Fig. 2(b). Then, there exists

$$\frac{1}{\lambda} = \frac{z(\mathbf{Q})}{{}^{c_z}z_p}, \quad (8)$$

and

$$z(\mathbf{Q}) = \frac{\mu + \sqrt{\mu^2 - (\xi^2 - 1)(\xi^2(q_1^2 + q_2^2) - \mu^2)}}{\xi^2 - 1}. \quad (9)$$

Thus, δ in Eq. (2) can be written as

$${}^c \mathbf{P}_p = \frac{{}^c z_p}{z(\mathbf{Q})} \begin{bmatrix} \mathbf{Q} \\ 1 \end{bmatrix}. \quad (10)$$

C. Kinematics

It is assumed that the mobile robots can be modeled by unicycles. As shown in Fig. 1, the inputs to each robot consist of one linear velocity and one angular velocity. The kinematic equation of the unified image-based leader-follower system is derived in this subsection.

Firstly, the kinematics of feature point P relative to follower frame will be derived. Without loss of generality, it is assumed that the feature point located at the origin of F_l . Then, the time derivative of the 3D coordinates of feature point P in the follower frame, *i.e.*, ${}^f \dot{\mathbf{P}}_p$, is

$${}^f \dot{\mathbf{P}}_p = \mathbf{J}_{ff} ({}^f \mathbf{P}_p) \mathbf{u}_f + \mathbf{J}_{ff}(\gamma) \mathbf{u}_l, \quad (11)$$

where $\mathbf{u}_i = [v_i, \omega_i]^T$, ($i=l, f$) denote the absolute linear velocity and angular velocity of the leader and follower. γ denotes the difference of orientations, as is shown in Fig. 1. The corresponding interaction matrices are denoted by \mathbf{J}_{ff} and \mathbf{J}_{ff} .

Next, the kinematics of the corresponding point in the unified camera frame can be derived based on Eq. (11). The mapping from ${}^f \mathbf{P}_p$ to coordinates in the camera frame ${}^c \mathbf{P}_p$ and from ${}^f \dot{\mathbf{P}}_p$ to ${}^c \dot{\mathbf{P}}_p$ are

$$\begin{bmatrix} {}^c \mathbf{P}_p \\ 1 \end{bmatrix} = ({}^f \mathbf{g}_c)^{-1} \begin{bmatrix} {}^f \mathbf{P}_p \\ 1 \end{bmatrix}, \quad {}^c \dot{\mathbf{P}}_p = ({}^f \mathbf{R}_c)^T {}^f \dot{\mathbf{P}}_p, \quad (12)$$

where ${}^f \mathbf{g}_c$ denotes the homogeneous transformation of F_c *w.r.t.* F_f . ${}^f \mathbf{R}_c$ denotes the corresponding rotation matrix. Replacing ${}^f \dot{\mathbf{P}}_p$ in Eq. (12) by Eq. (11) and ${}^c \dot{\mathbf{P}}_p$ yields

$${}^c \dot{\mathbf{P}}_p = \mathbf{J}_{fc} ({}^c \mathbf{P}_p) \mathbf{u}_f + \mathbf{J}_{fc}(\gamma) \mathbf{u}_l, \quad (13)$$

where \mathbf{J}_{fc} and \mathbf{J}_{fc} are interaction matrices.

Next, the kinematics of point P in the image plane, *i.e.*, ${}^l \mathbf{P}_p$, will be derived. According to Eq. (1), the time derivate of ${}^l \mathbf{P}_p$ is

$${}^l \dot{\mathbf{P}}_p = \frac{\partial \rho({}^l \mathbf{P}_p)}{\partial {}^c \mathbf{P}_p} {}^c \dot{\mathbf{P}}_p. \quad (14)$$

Substituting Eq. (13) into Eq. (14) and substituting ${}^c \mathbf{P}_p$ with Eq. (2) yields

$${}^l \dot{\mathbf{P}}_p = \underbrace{\frac{\partial \rho({}^l \mathbf{P}_p)}{\partial {}^l \mathbf{P}_p} \mathbf{J}_{fc} ({}^l \mathbf{P}_p, {}^c z_p)}_{\mathbf{J}_{fl}({}^l \mathbf{P}_p, {}^c \mathbf{P}_p)} \mathbf{u}_f + \underbrace{\frac{\partial \rho({}^l \mathbf{P}_p)}{\partial {}^l \mathbf{P}_p} \mathbf{J}_{fc}(\gamma)}_{\mathbf{J}_{ll}({}^l \mathbf{P}_p, {}^l \mathbf{P}_p, \gamma)} \mathbf{u}_l, \quad (15)$$

where \mathbf{J}_{fl} and \mathbf{J}_{ll} are interaction matrices. Equation (15) expresses the kinematic equation of the unified image-based leader-follower system. However, it contains the depth ${}^c z_p$ which is difficult to measure in the monocular case. But it is noted that all of ${}^c z_p$ in Eq. (15) are in the form of $1/{}^c z_p$.

Finally, the depth ${}^c z_p$ in Eq. (15) will be substituted by some measurable variables. According to the assumptions, the robots move in a plane. Thus, the feature point P moves in a fixed plane *w.r.t.* frame F_c , and this constraint is

$$a {}^c x_p + b {}^c y_p + c {}^c z_p = 1, \quad (16)$$

where a , b , and c are the coefficients of the plane equation. Then, $1/{}^c z_p = a/\lambda_1(y_1 - y_{1o}) + b/\lambda_2(y_2 - y_{2o}) + c$ can be obtained by considering the intrinsic parameters. Replacing $1/{}^c z_p$ in Eq. (15) results in

$${}^l \dot{\mathbf{P}}_p = \mathbf{H}({}^l \mathbf{P}_p) \mathbf{u}_f + \frac{\mathbf{G}({}^l \mathbf{P}_p, \gamma) \mathbf{u}_l}{\mathbf{F}({}^l \mathbf{P}_p, \gamma, v_l, \omega_l)}. \quad (17)$$

Thus, the final version of kinematic equation of the unified image-based leader-follower system is obtained in Eq. (17), which is independent of the depth ${}^c z_p$. This equation will be used in designing the controller in Section III.

Property 1: \mathbf{H} in Eq. (17) contains the uncertain constant parameters $\boldsymbol{\theta} \in \mathfrak{R}^n$, where n indicates the number of uncertain constant parameters. For any 2-dimension vector $\mathbf{u} \in \mathfrak{R}^2$, $\mathbf{H}(\boldsymbol{\theta}, {}^l \mathbf{P}_p) \mathbf{u}$ can be parameterized in a linear form as:

$$\mathbf{H}(\boldsymbol{\theta}, {}^l \mathbf{P}_p) \mathbf{u} = \mathbf{M}({}^l \mathbf{P}_p, \mathbf{u}) \boldsymbol{\theta}, \quad (18)$$

where $\mathbf{M}({}^l \mathbf{P}_p, \mathbf{u}) \in \mathfrak{R}^{2 \times n}$ is the known regressor matrix independent of the uncertain $\boldsymbol{\theta}$. This property will be used in designing the adaptive estimator in Section III.

In the case of perspective camera, the matrix $\mathbf{H}(\boldsymbol{\theta}, {}^l \mathbf{P}_p)$ is given by $\mathbf{H}_p(\boldsymbol{\theta}_p, \mathbf{y}_p)$, where $\boldsymbol{\theta}_p \in \mathfrak{R}^{16 \times 1}$ contain the intrinsic and extrinsic parameters of the camera and the coefficients of the plane equation: a , b and c . In the case of omnidirectional camera, the matrix $\mathbf{H}(\boldsymbol{\theta}, {}^l \mathbf{P}_p)$ in Eq. (18) is given by $\mathbf{H}_o(\boldsymbol{\theta}_o, \mathbf{Q})$, where $\boldsymbol{\theta}_o \in \mathfrak{R}^{21 \times 1}$ contain the extrinsic parameters of the camera and the coefficients of the plane equation: a , b and c .

III. ADAPTIVE UNIFIED IMAGE-BASED FORMATION CONTROL

In this section, an adaptive unified image-based leader-follower formation control scheme, including an image-based controller and an adaptive estimator, is proposed.

A. Controller and Estimator Design

Defined the error variable by $\mathbf{r} = \mathbf{k} \mathbf{e}_l + \boldsymbol{\Phi}$, with the image error $\mathbf{e}_l = {}^l \mathbf{P}_p - {}^l \mathbf{P}_{pd}$ and $\boldsymbol{\Phi} = [\Phi_1, \Phi_2]^T$. Since the desired relative position of the leader *w.r.t.* F_f is constant, the desired position of the feature point P on the image plane ${}^l \mathbf{P}_{pd}$ is constant. The image-based filter inspired by filters applied in [10] is introduced as

$$\dot{\boldsymbol{\Phi}} = -\mathbf{K}_3 \boldsymbol{\Psi} - \mathbf{K}_2 \mathbf{r}, \quad \boldsymbol{\Phi}(0) = \mathbf{0}_{2 \times 1}, \quad (19)$$

where $\boldsymbol{\Psi} = [\arctan \Phi_1 \quad \arctan \Phi_2]^T$. $\mathbf{k}, \mathbf{K}_2, \mathbf{K}_3 \in \mathfrak{R}^{2 \times 2}$ are positive-definite and diagonal gain matrices. The control goal is make sure \mathbf{e}_l approaches zero, and \mathbf{r} will be considered in the control loop in order to achieve the control goal.

An adaptive estimator, which generates estimated parameters $\hat{\boldsymbol{\theta}}$, is proposed as:

$$\frac{\partial \hat{\boldsymbol{\theta}}}{\partial t} = \Gamma_2^{-1} \mathbf{M}^T ({}^l \mathbf{P}_p, v_f, \omega_f) \mathbf{k} \Gamma_1 \mathbf{r}, \quad (20)$$

where the first term in Eq. (20) comes from the adaptive control theory [12] and *Property 1*. $\Gamma_2 \in \mathfrak{R}^{n \times n}$ and $\Gamma_1 \in \mathfrak{R}^{2 \times 2}$ are positive-definite and diagonal gain matrices. \mathbf{M}^T is known in the control process according to *Property 1*.

Depending on the estimated parameters $\hat{\boldsymbol{\theta}}$, the controller is

$$\mathbf{u}_f = (\mathbf{k}\hat{\mathbf{H}})^{-1}(-\mathbf{K}_1\mathbf{r} + \Gamma_1^{-1}\mathbf{K}_2\Pi + \mathbf{K}_3\Psi), \quad (21)$$

where $\Pi = [\tanh(\alpha_1\Phi_1) \quad \tanh(\alpha_2\Phi_2)]^T$. $\mathbf{k}\hat{\mathbf{H}}(\hat{\mathbf{\theta}}, \mathbf{y})$ are calculated using the estimated parameters $\hat{\mathbf{\theta}} \in \mathfrak{R}^{n \times 1}$. α_1 and α_2 are positive gains. $\mathbf{K}_1 \in \mathfrak{R}^{2 \times 2}$ are positive-definite and diagonal gain matrices. In practice, the control signal can be calculated by Eq. (21) using $\hat{\mathbf{\theta}}$ in each loop. The reason for the controller and estimator in this structure is they can guarantee a negative differential of the Lyapunov candidate equation, which will be shown below.

B. Stability Analysis

Theorem 1: Assume that the system satisfies the assumptions, and $\gamma(t_0) \neq \pm\pi$ and $v_l^f z_{pd} > 0$. With the controller proposed in Eq. (21) and the estimator presented in Eq. (20), the image-based leader-follower system is Uniform Semiglobal Practical Asymptotic Stability (USPAS).

Proof: Introduce the candidate Lyapunov equation as

$$V = \underbrace{\frac{1}{2}\mathbf{r}^T\Gamma_1\mathbf{r} + \mathbf{L}^T\Lambda\mathbf{L} + \frac{1}{2}\tilde{\mathbf{\theta}}^T\Gamma_2\tilde{\mathbf{\theta}} + \frac{1}{2}\gamma^2}_{V_1}, \quad (22)$$

where $\mathbf{L} = \begin{bmatrix} \sqrt{\ln \cosh(\alpha_1\Phi_1)} & \sqrt{\ln \cosh(\alpha_2\Phi_2)} \end{bmatrix}^T$, and $\Lambda = \text{diag}(\alpha_1^{-1} \quad \alpha_2^{-1})$ is a positive-definite and diagonal gain matrix.

First, the derivative of V_1 is

$$\dot{V}_1 = \mathbf{r}^T\Gamma_1\dot{\mathbf{r}} + (-\mathbf{K}_3\Psi - \mathbf{K}_2\mathbf{r})^T\Pi + \tilde{\mathbf{\theta}}^T\Gamma_2\dot{\tilde{\mathbf{\theta}}}, \quad (23)$$

where $\dot{\tilde{\mathbf{\theta}}} = \dot{\mathbf{\theta}} - \dot{\mathbf{\theta}}$. Next, it is shown that \dot{V}_1 is not greater than zero after plugging in the controller and estimator. Substituting Eq. (10) into the derivative of \mathbf{r} in Eq. (23) results in

$$\dot{\mathbf{r}} = \mathbf{k}\hat{\mathbf{H}}\mathbf{u}_f + \mathbf{kF} - \mathbf{K}_3\Psi - \mathbf{K}_2\mathbf{r} - (\mathbf{k}\hat{\mathbf{H}} - \mathbf{kH})\mathbf{u}_f, \quad (24)$$

which is called the open-loop kinematics. Then, consider the feedback loop in Eq. (24). Substituting the controller Eq. (21) into Eq. (24) and exploiting *Property 1* yields the closed-loop kinematic equation:

$$\dot{\mathbf{r}} = -\mathbf{K}_1\mathbf{r} - \mathbf{K}_2\mathbf{r} + \mathbf{kF} + \Gamma_1^{-1}\mathbf{K}_2\Pi - \mathbf{kM}\tilde{\mathbf{\theta}}. \quad (25)$$

Finally, substituting Eq. (25) and the estimator Eq. (20) into Eq. (23) yields

$$\begin{aligned} \dot{V}_1 &= -\mathbf{r}^T\Gamma_1(\mathbf{K}_1 + \mathbf{K}_2)\mathbf{r} + \mathbf{r}^T\Gamma_1\mathbf{kF} - \mathbf{K}_3\Psi^T\Pi, \\ &\leq -\mathbf{K}_3\Psi^T\Pi - \left[\lambda_{\min}(\Gamma_1\mathbf{K}_1 + \Gamma_1\mathbf{K}_2) - \frac{\lambda_{\max}(\Gamma_1\mathbf{k})\|\mathbf{F}(\mathbf{P}_p, v_l, \omega_l, \gamma)\|}{\|\mathbf{r}\|} \right] \|\mathbf{r}\|^2, \end{aligned} \quad (26)$$

where $\lambda_{\min}(\bullet)$ and $\lambda_{\max}(\bullet)$ denote the minimum and maximal eigenvalues of a positive-definite and diagonal gain matrix respectively. Denote the closed circles with radius σ_1 centered at the origin in \mathfrak{R}^2 by B_{σ_1} . The positive constant σ_2 denotes the radius of range centered at the origin in \mathfrak{R}^1 . Denote the upper bound of $\|\mathbf{F}(\mathbf{P}_p, v_l, \omega_l, \gamma)\|$ by f_{\max} . Then Eq. (26) can be calculated as follows:

$$\dot{V}_1 \leq - \left[\lambda_{\min}(\Gamma_1\mathbf{K}_1 + \Gamma_1\mathbf{K}_2) - \frac{\lambda_{\max}(\Gamma_1\mathbf{k})f_{\max}}{\|\mathbf{r}\|} \right] \|\mathbf{r}\|^2 - \mathbf{K}_3\Psi^T\Pi, \quad (27)$$

where $-\mathbf{K}_3\Psi^T\Pi$ is an odd function of Φ , so $-\mathbf{K}_3\Psi^T\Pi \leq 0$. There is an arbitrary small positive constant ℓ which can be regarded as the radius of a circle Ξ_1 centered at origin in \mathfrak{R}^2 ,

and there are \mathbf{K}_1 and \mathbf{K}_2 satisfying $\lambda_{\min}(\Gamma_1\mathbf{K}_1 + \Gamma_1\mathbf{K}_2) = (\lambda_{\max}(\Gamma_1)f_{\max})/\ell$, ℓ can be adjusted by \mathbf{K}_1 and \mathbf{K}_2 . For any $\mathbf{e}_l(0) \in B_{\sigma_1}$, $\gamma(0) \in B_{\sigma_2}$ and $\|\mathbf{r}\| > \ell$, the first term at the right-hand side of Eq. (27) is negative. Thus, $\dot{V}_1 < 0$ and $\mathbf{e}_l \in B_{\sigma_1}$, $\gamma \in B_{\sigma_2}$ and \mathbf{r} converges to the edge of Ξ_1 while ℓ can be adjusted by gains. Therefore, \mathbf{r} is Uniform Semiglobal Practical Asymptotic Stability (USPAS) [13]. Then, Φ and \mathbf{e}_l are all USPAS.

The differential of V_2 results in $\dot{V}_2 = \gamma\dot{\gamma}$. Because of the USPAS of \mathbf{e}_l , $({}^f x_p, {}^f z_p)$ converges to the desired $({}^f x_{pd}, {}^f z_{pd})$. Using kinematic model Eq. (11),

$$\dot{\gamma} = \omega_l - \omega_f = -\frac{v_l}{{}^f z_p} s_\gamma + \underbrace{\left(\frac{1}{{}^f z_p} ({}^f z_p + n_x s_\gamma - n_z c_\gamma) \omega_l + \frac{1}{{}^f z_p} {}^f \dot{x}_p \right)}_{\eta_1}, \quad (28)$$

where $s_\gamma = \sin \gamma$, $c_\gamma = \cos \gamma$. When $({}^f x_p, {}^f z_p)$ converges, the nominal system $\dot{\gamma} = -v_l / {}^f z_p s_\gamma$ can be expressed as $\dot{\gamma} = -v_l / {}^f z_{pd} s_\gamma$, and it is exponentially stable when $v_l^f z_{pd} > 0$ is satisfied. Due to the boundedness of ω_l , s_γ and c_γ , and the stability of ${}^f z_p$ and ${}^f \dot{x}_p$, $\|\eta_1\| \leq b_\eta$ is obtained. According to the stability of the perturbed system, when $\gamma(t_0) \neq \pm\pi$, the perturbed system Eq. (28) satisfies $\|\gamma\| \leq b_\gamma$, i.e., γ is bounded. b_η and b_γ are positive constant related to ${}^f z_{pd}$, $\bar{\omega}_l$.

In summary, Φ and \mathbf{e}_l are all USPAS, and γ is bounded. Therefore, the image-based leader-follower system is USPAS. ■

IV. EXPERIMENTS

Two mobile robots are used in the experiments and Fig. 3 (a) and (c) show the experimental system setup. An on-board camera is connected to a laptop with Pentium IV CPU. The low-level servo system can drive the wheels to achieve the desired velocity. The current velocity of the robot, required in the estimator, is calculated from the encoders on the wheels. There is no communication between robots, and the measurement or estimation of the absolute velocity of feature point is not necessary. The global visual positioning system (GVPS) is implemented to record the absolute positions of two robots in the experiments. It is noted that neither the controller nor the estimator depends on any global information. The GVPS is composed of two wide angle cameras fixed on the ceiling. The position, orientation, and ID information of robots can be recognized by the GVPS through the special marks mounted on the top of robots. The accuracy of the GVPS for position and orientation are ± 0.01 m and ± 0.02 rad.

A. Omnidirectional Camera

In the first two experiments, the omnidirectional camera is applied. The intrinsic parameters, i.e., matrix \mathbf{A} , ξ and μ , are known. The extrinsic parameters of the omnidirectional camera and the coefficients of the plane where feature point P moves relative to the camera frame, i.e., a , b , and c , are uncertain. Fig. 3(b) shows an image from the omnidirectional camera. The threshold image segmentation is used to detect

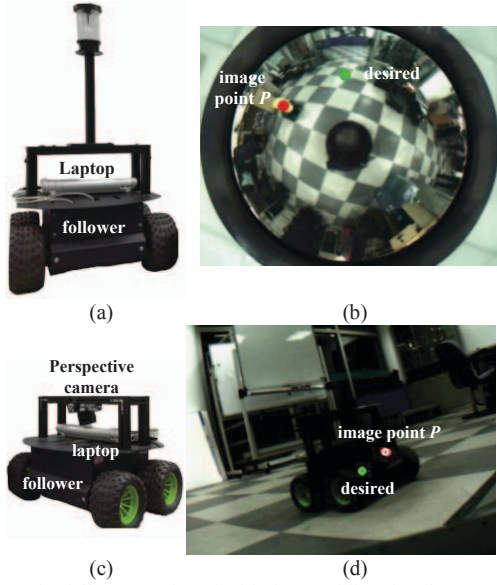


Fig. 3. (a) The follower equipped with the omnidirectional camera, (b) the image from the omnidirectional camera, (c) the follower equipped with the perspective camera, and (d) the image from the perspective camera.

the center of a yellow cylinder on the leader, *i.e.*, y_o , from the image. The visual processing period is 64ms. Then, Q is calculated based on Eq. (6).

The camera is positioned upright and the 3D coordinate of the origin of F_c w.r.t. F_f were roughly measured as $(m_x = 0.1\text{m}, m_y = -0.3\text{m}, m_z = 0.1\text{m})$. The height of the point from the origin of F_c is approximately 0.3 m. Thus, the true values of θ_o are uncertain. The initial values of $\hat{\theta}_o$ were selected around the roughly measured values. The initial estimated parameters are $\hat{\theta}_o(t_0) = [0, 0, 0, 0, 0, 2, 0, 0, 0, 0, 0, 0, 0, 0, 0, 0, 0, 0, 2]^T$. The gain matrices are $\mathbf{K}_1 = \text{diag}(10, 10)$, $\mathbf{K}_2 = \text{diag}(6, 6)$, $\mathbf{K}_3 = \text{diag}(0.1, 0.1)$, $\Gamma_1 = \text{diag}(1, 1)$, $\Gamma_2 = 10^{-4} \mathbf{I}_{21 \times 21}$, $\mathbf{k} = \text{diag}(0.5, 0.5)$, $\alpha_1 = 3$ and $\alpha_2 = 3$. The suitable gains are determined in the experiments.

In the first experiment, the leader moved in a linear trajectory at 0.25 m/s. The desired relative position is $({}^f x_{pd}, {}^f z_{pd}) = (0, 1)$ m, and the corresponding desired point in the image plane is $(y_{o1d}, y_{o2d}) = (283, 117)$ pixel. Figure 4 (a) shows the trajectory of the feature point in the omnidirectional image plane. Figure 4(b) shows the convergence of the image error Δy_{o1} and Δy_{o2} . Figure 4 (c)-(f) shows parts of the estimated parameters due to the limits on the length of the paper. They varied resulting from the image error. According to Section III.B, the errors $\tilde{\theta}_o$ decrease at the beginning, but the convergence stops when the image errors approach zero. At this time, $\hat{\theta}_o$ may not converge to the true values, but it does not obstruct the convergence of the image errors.

In the second experiment, the leader moves in a circle at 0.2 m/s and 0.1 rad/s. $({}^f x_{pd}, {}^f z_{pd}) = (-0.2, 1)$ m and $(y_{o1d}, y_{o2d}) = (249, 126)$ pixel. Figure 5(a) shows the trajectory of the feature point in the omnidirectional image plane. Figure 5(b) shows the convergence of the image error.

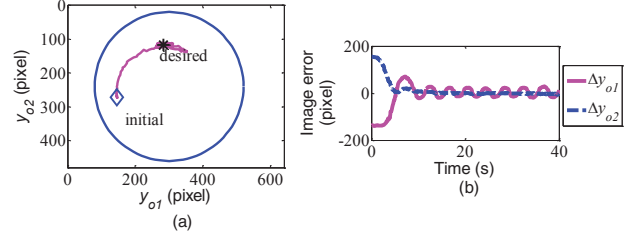


Fig. 4. The 1st exp. result: (a) image trajectory (b) image error.

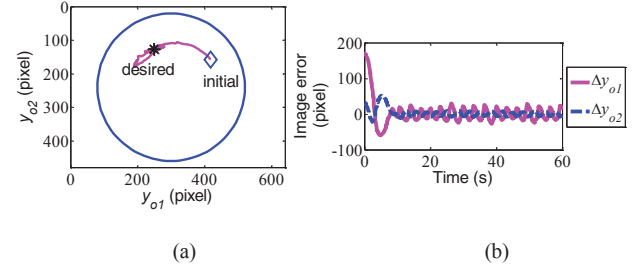


Fig. 5. The 2nd exp. result: (a) image trajectory and (b) image error.

B. Perspective Camera

In the last two experiments, the follower with a perspective camera is controlled to validate the proposed algorithm. The intrinsic and extrinsic parameters of the perspective camera and the coefficients of the plane where feature point P moves relative to the camera frame, *i.e.*, a , b , and c , are uncertain. Figure 3(d) shows an image from the perspective camera. To make the case more general, the obvious yellow cylinder is removed from the leader. The window-based BRISK keypoint detector [14] is utilized to detect 5 best matched keypoints on the leader through a sample picture. The average of their coordinates is y_p . The visual processing period is 50 ms.

The intrinsic and extrinsic parameters were roughly calibrated, where $\lambda_1 = 656$, $\lambda_2 = 656$, $y_{1o} = 301$, and $y_{2o} = 238$. The z - y - z rotation angles from F_f to F_c is $\varphi_1 = 0.17$ rad, $\varphi_2 = 0$ rad, $\varphi_3 = 0$ rad, $m_x = 0$ m, $m_y = 0$ m, and $m_z = 0.1$ m. The height of the point from the origin of F_c is approximately 0.1 m. The initial estimated parameters are selected based on the uncertain values. The differences between them were θ_p e Δy_{o2} more than 50% to 100% of roughly measured. $\hat{\theta}_p(t_0) = [1, 1, -0.015, 0.004, -1000, -1, 0, 0, 0.001, 1000, -1, 10, -1000, -0.1, -0.1, 100]^T$. The gains are selected as $\mathbf{K}_1 = \text{diag}(5, 5)$, $\mathbf{K}_2 = \text{diag}(10, 10)$, $\mathbf{K}_3 = \text{diag}(0.02, 0.02)$, $\Gamma_1 = \text{diag}(1, 1)$, $\Gamma_2 = \text{diag}(10^{-5}, 10^{-5}, 10^{-10}, 10^{-10}, 10^{-3}, 10^{-7}, 10^{-10}, 10^{-11}, 10^{-12}, 10^{-3}, 10^{-7}, 10^{-5}, 10^{-3}, 10^{-7}, 10^{-7}, 10^{-3})$, $\mathbf{k} = \text{diag}(0.1, 0.1)$, $\alpha_1 = 3$ and $\alpha_2 = 3$.

In the third experiment, the leader moved in a linear trajectory at 0.1 m/s, where $({}^f x_p, {}^f z_p) = (0, 1)$ m and $(y_{p1d}, y_{p2d}) = (303, 145)$ pixel. Figure 6(a) shows the straight trajectory of the feature point on the image plane. The image point reached its desired position following a straight line without leaving the field of view. Figure 6(b) shows the

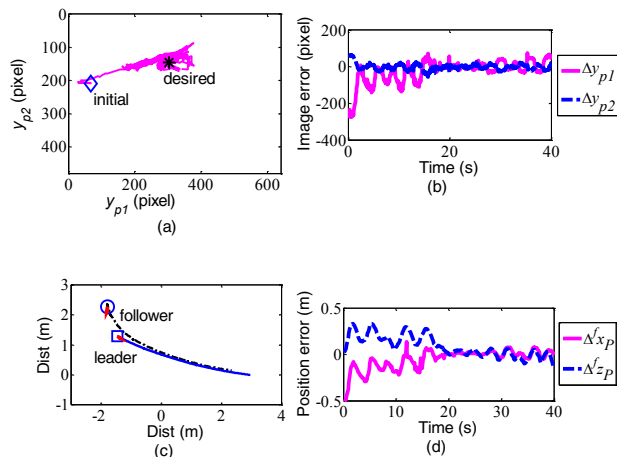


Fig. 6. The 3rd exp. results: (a) image trajectory, (b) image error, (c) the trajectory of two robots, and (d) position error in F_f .

convergence of the image error Δy_{p1} and Δy_{p2} . Figure 6(c) shows the smooth trajectory of two robots recorded by the GVPS. Figure 6(d) shows the convergence of the position error $\Delta^f z_p = {}^f z_p - {}^f z_{pd}$ and $\Delta^f x_p = {}^f x_p - {}^f x_{pd}$ recorded by the GVPS. In the fourth experiment, the leader moved along a circular trajectory at 0.2 m/s and 0.1 rad/s. $({}^f x_p, {}^f z_p) = (0, 1)$ m and $(y_{p1d}, y_{p2d}) = (303, 145)$ pixel. Similarly, Fig. 7 shows the results. The robustness of the control algorithm against noise is verified in the 3rd and 4th experiments. Under the poor performance of the detection, the system was still stable.

In summary, the proposed algorithm guarantees the convergence of the image errors at different initial values. The feature point on the leader can be tracked by the visual servo system at all times even under poor performance of the detection. Unfortunately, the tracking performance along the Z_f direction in the 4th experiment is not good because the perspective camera is not sensitive to the motion normal to the viewing plane.

V. CONCLUSION

This paper proposed an adaptive unified image-based control scheme for leader-follower formation control. Both omnidirectional and perspective cameras are suitable for the scheme. The camera parameters can be uncertain and communication between robots is not required. The image-based controller is independent of the velocity of the leader. The estimator can estimate the uncertain camera parameters, as well as the uncertain coefficients of the plane where the feature point moves in the camera frame. Based on the Lyapunov method, the proposed system is USPAS. Experimental results validate the performance of the proposed algorithm. Future work includes the design of the dynamic controller for the image-based leader-follower system.

REFERENCES

[1] A. K. Das, R. Fierro, V. Kumar, J. P. Ostrowski, J. Spletzer, and C. J. Taylor, "A vision-based formation control framework," *IEEE Trans. Robotics and Automation*, vol. 18, no. 5, pp. 813–825, 2002.

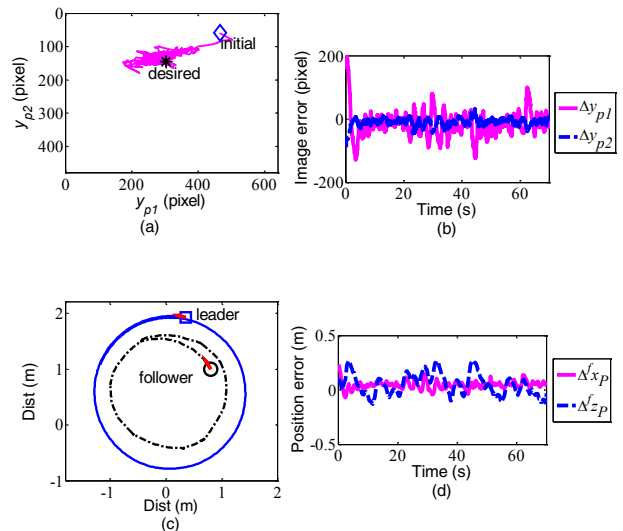


Fig. 7. The 4th exp. results: (a) the real trajectory in, (b) image error, (c) the trajectory of two robots, and (d) position error in F_f .

- [2] H. Poonawala, A. C. Satici, N. Gans, and M. W. Spong, "Formation control of wheeled robots with vision-based position measurement," in *Proc. IEEE Conf. American Control*, pp. 3173–3178, 2012.
- [3] X. Liang, Y. H. Liu, H. Wang, W. Chen, K. Xing and T. Liu, "Leader-Following Formation Tracking Control of Mobile Robots Without Direct Position Measurements," *IEEE Trans. on Automatic Control*, vol. 61, no. 12, pp. 4131–4137, 2016.
- [4] R. Vidal, O. Shakernia, and S. Sastry, "Formation control of nonholonomic mobile robots with omnidirectional visual servoing and motion segmentation," in *Proc. IEEE Int. Conf. Robotics and Automation*, vol. 1, pp.584–589, 2003.
- [5] H. Wang, S. Itani, T. Fukao, and N. Adachi, "Image-based visual adaptive tracking control of nonholonomic mobile robots," in *Proc. IEEE/RJS Int. Conf. Intelligent Robots and Systems*, vol. 1, pp. 1–6, 2001.
- [6] G. L. Mariottini, F. Morbidi, D. Prattichizzo, N. Vander Valk, N. Michael, G. Pappas, and K. Daniilidis, "Vision-based localization for leader–follower formation control," *IEEE Trans. Robotics*, vol. 25, no. 6, pp.1431–1438, 2009.
- [7] F. Morbidi, G. L. Mariottini, and D. Prattichizzo, "Observer design via immersion and invariance for vision-based leader–follower formation control," *Automatica*, vol. 46, no. 1, pp. 148–154, 2010.
- [8] H. Wang, D. Guo, X. Liang, W. Chen, G. Hu, and K. K. Leang, "Adaptive Vision-Based Leader-Follower Formation Control of Mobile Robots," *IEEE Trans. Industrial Electronics*, 2016.
- [9] D. Guo, W. Yim, and K. K. Leang, "Adaptive repetitive visual-servo control of a low-flying unmanned aerial vehicle with an uncalibrated high-flying camera," in *Proc. IEEE/RJS Int. Conf. Intelligent Robots and Systems*, pp. 4258–4265, 2016.
- [10] S. Purwar, I. N. Kar, and A. N.Jha, "Adaptive output feedback tracking control of robot manipulators using position measurements only," *Expert systems with applications*, vol. 34, no. 4, pp. 2789–2798, 2008.
- [11] C. Geyer and K. Daniilidis, "A unifying theory for central panoramic systems and practical applications," in *Proc. European Conf. Computer Vision*, pp. 445–461, 2000.
- [12] H. Wang, B. Yang, Y. Liu, W. Chen, X. Liang and R. Pfeifer, "Visual Servoing of Soft Robot Manipulator in Constrained Environments with an Adaptive Controller", *IEEE/ASME Trans. on Mechatronics*, vol. 22, no. 1, pp. 41–50, 2017.
- [13] A. Chaillet and A. Lorr'a, "Uniform semiglobal practical asymptotic stability for non-autonomous cascaded systems and applications," *Automatica*, vol. 44, no. 2, pp. 337–347, 2008.
- [14] S. Leutenegger, M. Chli, & R. Y. Siegwart, "BRISK: Binary robust invariant scalable keypoints," in *Proc. IEEE Int. Conf. Computer Vision*, pp. 2548–2555, 2011.